

Sonochemical synthesis, structural inspection and semiconductor behavior of three new nano sized Cu(II), Co(II) and Ni(II) chelates based on tri-dentate NOO imine ligand as precursors for metal oxides

Laila H. Abdel Rahman¹ | Ahmed M. Abu-Dief¹  | Rafat M. El-Khatib¹ |
Shimaa Mahdy Abdel-Fatah¹ | A.M. Adam² | E.M.M. Ibrahim²

¹Chemistry Department, Faculty of Science, Sohag University, 82534 Sohag, Egypt

²Physics Department, Faculty of Science, Sohag University, 82534 Sohag, Egypt

Correspondence

Ahmed M. Abu-Dief, Chemistry Department, Faculty of Science, Sohag University, 82534 Sohag, Egypt
Email: ahmed_benzoic@yahoo.com

Three novel nanosized Cu(II), Co(II) and Ni(II) complexes of imine ligand attained from the condensation of 2-amino-3-hydroxypyridine and 3-methoxysalicylaldehyde have been prepared and investigated using diverse chemical methods such as NMR, CHN analysis, conductance, IR, Spectral studies, TGA and magnetic moment measurements. The obtained data confirmed that the synthesized complexes have metal: ligand ratio of 1:1 and octahedral geometry for Co(II) and Ni(II) complexes. Interestingly, The complexes are used as precursors for producing CuO, Co₂O₃ and NiO nanoparticles by calcination at 500 °C and their structures were described by powder x-ray and transmittance electron microscopy. Furthermore, to investigate the feasibility of using the synthesized materials for semiconductor based nanodevices, the electrical properties of the prepared imine complexes and their corresponding metal oxides were investigated by measuring the electrical conductivity over a temperature range 373-593 K. The data confirm that the materials are semiconductor. The electrical conduction process in the complexes is governed by intermolecular and intramolecular transfer of the charge carriers. But, the conduction mechanism arises from the contribution of the phonon-assisted small polaron hopping in NiO nanoparticles and charge carrier hopping in CuO and Co₂O₃ nanoparticles. The results indicate that the complexes under study are promising candidates for wide scale of organic based semiconducting devices.

KEYWORDS

electrical properties, imines, nanoparticles, semiconductor, sonochemistry, thermal analyses

1 | INTRODUCTION

Transition metal compounds with Schiff base have been amid the most vastly investigated coordination compounds of the past few years, since they are found to be widely applicable in many domains such as biochemical

fields.^[1-5] Recently, there is great attention for preparation and description of novel nanosized semiconducting organic compounds for several novel technologies. When the size of semiconductor matters is decreased to nano-scale, their physic- chemical properties alter significantly, resulting in unique properties due to their high surface

area. Although, appearance of many nanosized semiconducting organic compounds is still in the research field, some are committed for applications in different fields, like solar cells, nanoscale electronic instruments, light-emitting diodes, laser technology, waveguide, chemical and biosensors, packaging films, superabsorbents and catalysts.^[6] In particular, Imine compounds could conduct as photostabilizers, dyes for solar collectors, solar filters due to their photochromic characteristics. They are also extended in optical sound recording technology.^[7,8]

Also, transition metal oxide nanoparticles represent a great class of materials that have been investigated extensively. Several methods have been reported in order to synthesize TMOs nanoparticles, including hydrothermal route, thermal degradation, sonochemical route.^[9,10] Transition metal oxides have gained great attention because of their great applications in optoelectronic devices made from organic semiconductors.^[11,12] For example, in organic light-emitting diodes, they are used as anode modification interlayers,^[13–15] which can substantially reduce the hole injection barrier. They are also opener components of charge generation layer in tandem organic light-emitting diodes. In organic solar cells, they are employed as charge extraction interlayer and recombination layer. Besides, transition metal oxides have many unique properties, such as high work function, semiconducting and good transparency, that are all very important for electrode interlayers and/or as charge generation/recombination matters. Among these characteristics, the high work function is the main reason for efficient operation of transition metal oxides based functional layers.^[16–18]

From this point of view, the aim of this research is to prepare an imine derived from 2-amino-3-hydroxypyridine and 3-methoxysalicylaldehyde and its Cu(II), Co(II) and Ni(II) complexes in nanometer size. Furthermore, the prepared nano-sized complexes were used as starting materials for preparation of Cu, Co and Ni oxide nanoparticles. Moreover, a comprehensive study has been presented about the electrical properties of the synthesized imine complexes and metal oxides with focus on the conduction mechanisms governing their electrical properties.

2 | EXPERIMENTAL

All the utilized matters of chemicals in this paper such as 3-methoxysalicylaldehyde (97%), 2-amino-3-hydroxypyridine (98%), the metal salts (Copper(II) acetate (98%), Cobalt(II) nitrate hexahydrate (98%) and Nickel(II) nitrate hexahydrate (98.5%)) were got from Sigma-Aldrich Chemie, Germany. Spectroscopic grade ethyl alcohol, dimethylformamide and HCl products were utilized.

2.1 | Synthesis of the investigated imine ligand

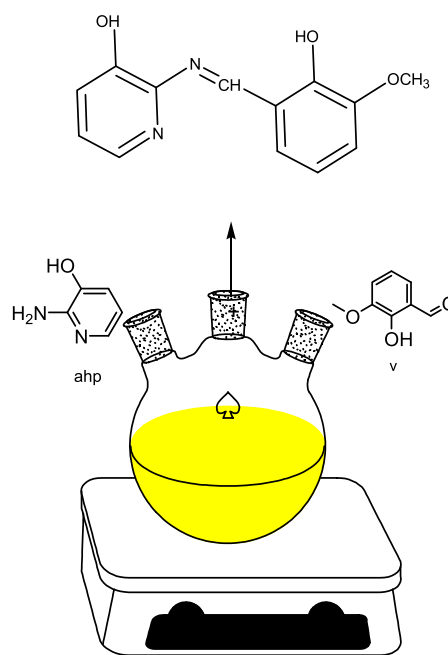
The imine ligand was synthesized by the condensation of 3-methoxysalicylaldehyde (0.304 g, 2 mmol) and 2-amino-3-hydroxypyridine (0.22 g, 2 mmol) (1: 1 molar ratio), dissolved in 20 ml ethyl alcohol. The mixture was refluxed for 1 h. The progress and the purity of the prepared ligand was checked by TLC. The orange precipitate of imine obtained was filtered, scrubbed with distilled water, desiccated, recrystallized from ethanol and kept in a desiccator (yield: 88%) as shown in (Scheme 1).

2.2 | Preparation of Cu(II), Co(II) and Ni(II) complexes with nano-compositions by sonochemical technique

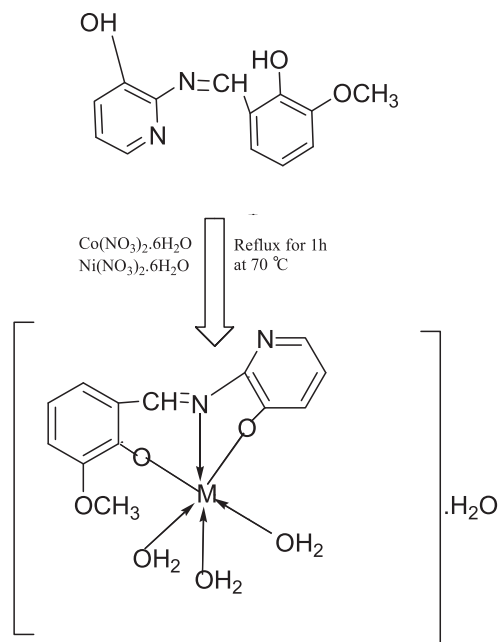
Forty milliliters of a 0.4 M ethyl alcohol solution of the different metal salts [(Copper acetate, 0.796 g), (Cobalt (II) nitrate hexahydrate, 1.16 g) and (Nickel nitrate hexahydrate, 1.16 g)] was placed in an ultrasonic probe, operating with a maximum force output of 400 W. Into this solution, 40 ml of 0.4 M solution of the LH₂ ligand (1.04 g) was added drop wise. The formed precipitate was filtered off, scrubbed with ethyl alcohol and then desiccated in air (yield: 75–84%) as shown in (Scheme 2).

2.3 | Preparation of nano-sized metal oxides from their corresponding complexes

Nano-sized metal oxides were got by calcination of (0.1 g) of the various complexes in air at 500 °C with a heating



SCHEME 1 synthesis of Schiff base ligand (LH₂), where ahp = 2-amino-3-hydroxypyridine and v = 3-methoxysalicylaldehyde



SCHEME 2 The suggested structures of LNi, LCo complexes

average 10 °C min⁻¹.^[19] The attained metal oxide is scrubbed with ethyl alcohol and dried in desiccator. The nano-scale compounds were characterized by transition electron microscopy and powder x-ray.

2.4 | Physical characterizations

Melting point of the imine ligand and degradation temperatures of the synthesized complexes were predestined utilizing a melting point tool, Gallenkamp, England, UK. Infra-Red spectra of the acquired compounds were patent by Shimadzu FTIR model 8101 spectrophotometer in KBr granules in the domain of 4000-400 cm⁻¹. Conductivity measurements were achieved by JENWAY conductivity meter model 4320 at room temperature plying DMF dimethylformamide as solvent. UV-Vis spectra in dimethylformamide were patent utilizing PG spectrophotometer model T+80. Proton NMR and Carbon-13 NMR spectra were procured by BRUKER NMR model 400 MHz plying dimethylsulfoxide-*d*₆ as the solvent. The offered imine ligand and its complexes were undergone to (C, H and N) analyses plying Elemental analyzer Perkin-Elmer (240c). The magnetic measurements were anticipated by Gouy's balance route. Shimaduz corporation 60H analyzer was anticipated for doing the thermogravimetric test under nitrogen with a heating average 10 °C min⁻¹. The values of absorbance of 5 × 10⁻³ M for complexes were measured at assorted pH levels. The pH levels were checked by plying a series of Britton global buffers.^[20,21] The pH was measured plying HANNA 211 pH meter at room temperature. The morphology of the matters was sought by transmission electron microscope

(TEM-2100). An ultrasonic generator (Dr. Hielscher UP400 S ultrasonic processor) equipped with a 'H22' sonotrode with diameter 22 mm was plied for the ultrasonic irradiation. The internal construction was sought using x-ray diffractometer: model X'pert3-Powder made by PAnalytical with monochromatized CuK α radiation. Particle size distribution of the synthesized imine complexes and their corresponding metal oxides was estimated utilizing image J Lanucher, broken-symmetry software, version (1.4.3.6.7).

2.5 | Electrical properties

To inspect the electrical characteristics of the synthesized imine complexes and metal oxides, the temperature (T) reliance of the electrical resistivity (ρ) by the so called two prop technique within temperature domain 373-593 K was inspected. DC electrical resistance of the specimen grains was standardized plying KEITHLEY 614 Electrometer, operating in the steady current pattern.^[22] The electrical resistivity (ρ) is defined as:

$$\rho = RA/d \quad (1)$$

Where R is the electrical resistance of an even specimen of the matter (measured in ohms, Ω), d and A are the thickness and cross-sectional area of the taking.

3 | RESULTS AND DISCUSSION

3.1 | Physical and chemical characteristics

All the synthesized complexes are variegated, tough, fixed at room temperature and non-hygroscopic in kind. The analytical and physicochemical data of ligand and its complexes are patent in (Table 1). The metal complexes manifested 1:1 (metal-ligand) ratio.

3.2 | ¹H-NMR and ¹³C-NMR spectra

The Proton NMR spectra of the LH₂ ligand manifests signals at 6.85-8.00 (m) δ for aromatic protons and 9.44(s) δ for azomethine proton. The peak at 10.28(s) δ is imputed to -OH group and it vanished upon addendum of D₂O. The peak at 3.34(s) δ is attributed to methoxy group. The Carbon-13 NMR offers the signals coincide to assorted non-equivalent carbon atoms at assorted values of δ as follows: at δ 169 ppm(CH=N) due to azomethine and at δ 122-156 ppm(11CH-Ar) due to aromatic carbon atoms. Also a signal evidences at δ 56 ppm(OCH₃) due to carbon atom of -OCH₃ group.^[23]

TABLE 1 The analytical and physical data of ligand and its metal complexes

Compound	Colour	(M.p) and Dec. ° C	M. Wt	Elemental analysis found(calculated)			Conductance Λ m (Ω^{-1} cm ² mol ⁻¹)	μ_{eff} B.M.
				C	H	N		
LH ₂	Orange	250	260	60.00 (60.15)	4.61 (4.71)	10.76 (10.64)	3.67	-
LCu	Light green	>300	341.5	45.68 (45.53)	4.09 (4.22)	8.19 (8.05)	6.75	2.07
LCo	Brick red	290	372.9	41.83 (41.70)	4.82 (4.89)	7.50 (7.65)	6.69	4.83
LNi	Brown	>300	372.7	41.85 (41.77)	4.82 (4.73)	7.51 (7.65)	4.76	3.69

3.3 | Infrared spectra

The Infra-Red hesitations of the LH₂ ligand and its complexes along with their assignments are manifested in (Table S1). Bands due to -OH and -CH=N are discernible and bid proof respecting the structure of the ligand and its bonding with metal. A band at 1613 cm⁻¹ in the imine ligand is due to -C=N stretching vacillation. On complexation, this band is dislodged to a down hesitation. The negative shift of this band is an obvious marker of the participation of the azomethine nitrogen atoms in complex consistence.^[1,2,9,20,21,24-26] This is supported by the manifesting of band at 527-535 cm⁻¹ coinciding to the stretching vacillation of M-N bond. The bands subsist at 732-736 cm⁻¹ coincide to the M-O stretching vacillations. The band manifests at 3447 cm⁻¹ spotted in the ligand spectrum is due to stretching vacillations of free -OH. In the complexes, the patent Infra-Red spectra of all the synthesized complexes manifest wide band at 3450-3510 cm⁻¹ which have been assigned to $\nu(\text{OH})$ stretching vacillation of hydrated water molecules, in accordance with the findings of the CHN analysis patent in (Table 1). A band at 968-976 cm⁻¹ (OH rocking) proposes the subsist of coordinated water in all three complexes. In the low hesitation zone, the band spotted for imine ligand manifested an absorption band at 1307 cm⁻¹ which can result from the stretching vacillation of the phenolic (C-O) group.^[28] The stir of that band to lower wave number values upon complexation manifests that the oxygen atoms of the phenolic groups are bonded to the metal ion. The bands notified in the zones 3011-3100 cm⁻¹ can be assigned to $\nu(\text{C-H})$ aromatic stretching vacillations.^[1,2,4,5]

3.4 | Electronic spectra

The molecular electronic absorption spectra are often very leading for affirming the results attained by other techniques of structural inspection. The electronic spectral measurements were performed for specifying the stereo chemistries of metal ions in the complexes reliance on the sites and number of *d-d* transition peaks.^[29] The

electronic absorption spectra of the ligands and their complexes were patent at the wavelength domain 800-200 nm and at temperature of room temperature. The ligand manifests absorption bands in UV-Vis zone around 355 nm which is assigned to $n \rightarrow \pi^*$ transition creating from the imine group.^[30] The absorption bands of complexes at $\lambda_{\text{max}}=391-414$ nm is assigned to charge transfer in imine ligands. Furthermore, an intense and broad band lies in the zone 430-455 nm ($\epsilon_{\text{max}}=1240-850$ mol⁻¹ cm²). This band could be mainly attributed to the $d \rightarrow d$ transition in the structure of the prepared complexes (Figure S1).^[31]

3.5 | Magnetic moment measurements

In the paramagnetic matters, the magnetic moments are aligned in the effected magnetic field direction. Therefore, the paramagnetic matters own positive susceptibilities. Thus, the magnetic susceptibility measurements manifest information on regard the geometric structure of the compounds. Magnetic susceptibility measurements manifested that all the prepared complexes have paramagnetic property and octahedral geometry barring copper complex which has tetrahedral geometry.^[23,28,32]

3.6 | Thermal analysis

The thermograms of Copper, Cobalt and Nickel complexes affirm the subsisting of one molecule of coordinated water in case of copper and three coordinated water molecules in case of Cobalt and Nickel complexes.^[33] The thermal mode of the metal complexes manifested that the hydrated complexes forfeit water molecules of hydration in the first stage; then liberation coordinated water molecules with degradation of the ligand molecules in the subsequent stages as manifested in (Table S2) and Figures (1,2). The LCu, LCo and LNi have weight forfeits of 5.11, 4.85 and 4.78 %, respectively, which are due to sweep of water molecules of hydration. The weight forfeits of 27.48 and 48.11% coincide to the sweep of the remaining thermally degradable fraction of

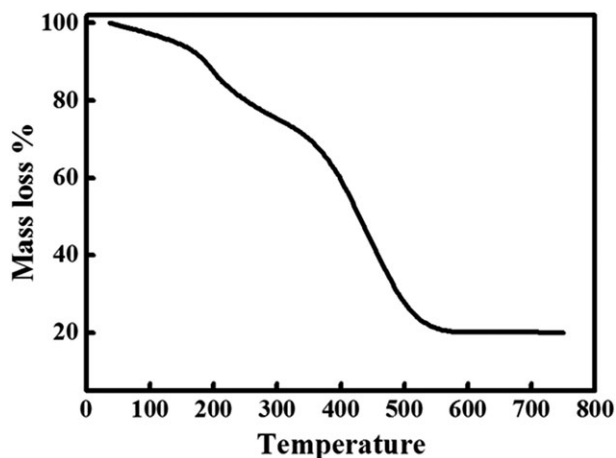


FIGURE 1 TGA curve of LCu complex

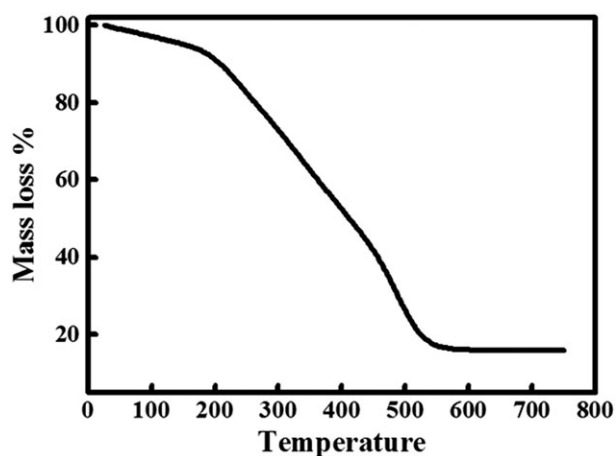


FIGURE 2 TGA curve of LCo complex

the complex at temperature domain 155.3-501.0 °C with respect to LCu complex. The weight forfeits of 22.82, 24.03 and 32.39% coincide to the sweep of the remaining thermally degradable portion of the complex at temperature domain 153.5-522.8 °C with respect to LCo complex. The weight forfeits of 22.91, 31.51 and 24.83% coincide to the sweep of the remaining thermally degradable portion of the complex at temperature domain 166.1-479.9 °C with respect to LNi complex. The eventual product explained from a horizontal curve has been attained suggesting consistence of metal product.^[33,34]

3.7 | Kinetic aspects

The thermodynamic parameters of the degradation operations of the complexes were calculated plying the Coasts-Redfern equation,^[35,36]

$$\log \left[\frac{\log(w_{\infty} - w)}{T^2} \right] = \log \left[\frac{AR}{\varphi E^*} \left(1 - \frac{2RT}{E^*} \right) \right] - \frac{E^*}{2.303RT} \quad (2)$$

Where W_{∞} is the mass forfeit at the completion of the degradation process. W is the mass perishing up to temperature T , R is the gas constant and φ is the heating average. Since $(1 - 2RT/E^*) \approx 1$, the plot of the left side of equation versus $1/T$ would offer a straight line. E^* was then predestined from the slope and the Arrhenius constant, A , was profited from the intercept. The other kinetic parameters; the entropy of activation (S^*), enthalpy of activation (H^*) and the free energy variance of activation (G^*) were predestined using the following equations:

$$S^* = 2.303R \log \frac{Ah}{kT} \quad (3)$$

$$H^* = E^* - RT \quad (4)$$

$$G^* = H^* - TS^* \quad (5)$$

Where (k) and (h) are Boltzmann's and Plank's constants, respectively. The Kinetic parameters are manifested in (Table S3). It can be manifested that G^* values boosts with the growth of temperature. The positive values of H^* manifest that degradation operations are endothermic. In most thermal stages, S^* values are negative proposing a decomposition via abnormal passing at those stages and the degradation operations are unfavorable. The negative activation entropy value proposes that the activated complexes are more ordered than the reactant and the reactions are overdue. The more ordered kind is attributed to the polarization of bonds in the activated state which might procure through charge transfer electronic transitions. Finally, positive values were offered for H^* and G^* respectively representing endothermic character for all thermal stages.^[37]

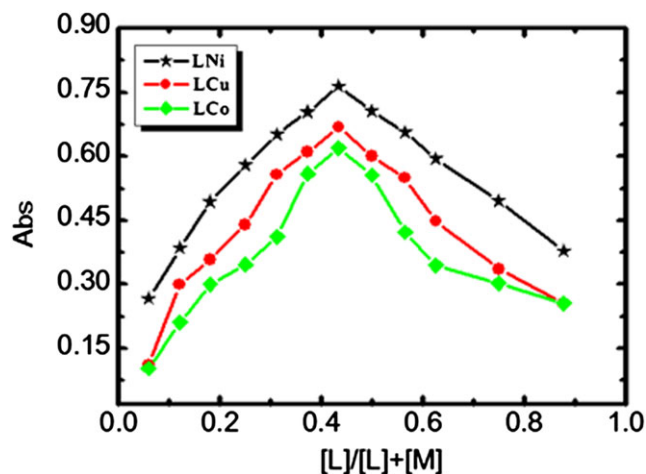


FIGURE 3 Continuous variation plots for the prepared complexes in aqueous-alcoholic mixtures at $[M] = [L] = 1 \times 10^{-3}$ M and 298 K

3.8 | Spectrophotometric estimation of the stoichiometry of the prepared complexes

Stoichiometry of the synthesized complexes is predestined plying the two techniques encompassing the utilize of spectrophotometry, namely, continuous-variations route and mole-ratio route. Reliance on the methods plied and the experimental conclusion, the stoichiometry of the synthesized complexes is 1:1. The curves of the continuous variation technique (Figure 3) offered maximum absorbance at mole fraction $X_{\text{ligand}} = 0.5-0.6$ manifesting the complexation of metal ions to ligand in molar ratio 1:1. Moreover, the data resulted from applying the molar ratio route prop the same metal to ligand ratio of the prepared complexes (Figure S2).^[38–41]

3.9 | Estimation of the apparent formation constants of the synthesized complexes

The consistence constants (K_f) of the studied imine complexes consisted in solution were attained from the spectrophotometric measurements by plying the continuous variation route (Table 2) according to the following equation^[32,36,37]:

$$K_f = \frac{A/A_m}{4C^2(1-A/A_m)^3} \quad (6)$$

Where, A_m is the absorption at the maximum consistence of the complex, A is the arbitrary selected absorbance values on either hand of the absorbance mountain col (pass) and C is the incipient concentration of the metal. As acquired in (Table 2), the attained K_f values manifest the great constancy of the synthesized complexes. The values of K_f for the synthesized complexes enhance in the following order: $\text{LCo} > \text{LNi} > \text{LCu}$. Moreover, the amount of the constancy constant (pK) and Gibbs free energy (ΔG^\ddagger) of the complexes under study are predestined. The negative amount of Gibbs free energy means that the reaction is spontaneous and favored. The pH-profile manifested in Figure 4 show perfect dissociation curves and a high constancy pH extent (4–9) of the tested complexes. This shows that the consistence of the complex greatly stabilizes the imine ligands. Consequently, the suitable pH domain for the different applications of the tested complexes is from pH = 4 to pH = 9. Based on the data of CHN analyses, conductance, magnetic susceptibility, infrared and electronic spectra, the suggested composition of the complexes was described.

TABLE 2 The formation constant (K_f), stability constant (pK) and Gibbs free energy (ΔG^\ddagger) values of the synthesized complexes in aqueous-ethanol at 298 K

Complex	Type of complex	K_f	pK	ΔG^\ddagger kJ mol ⁻¹
LCu	1:1	7.15×10^8	8.85	-50.48
LCo	1:1	1.10×10^{10}	10.04	-57.25
LNi	1:1	9.60×10^9	9.98	-56.91

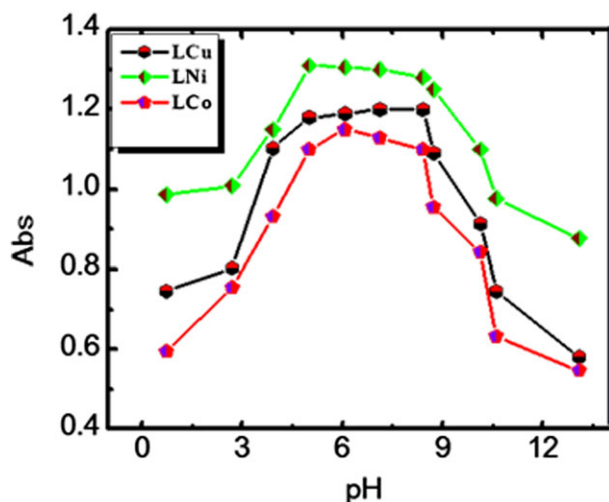


FIGURE 4 Dissociation curves of the prepared complexes in aqueous alcohol mixtures at $[M] = [L] = 1 \times 10^{-3}$ M and 298 K

3.10 | TEM and XRD of the prepared complexes and metal oxides

The Cobalt, Copper and Nickel oxides nanoparticles were synthesized at 500 °C utilizing imine complexes as starting materials and their properties studied with the relief of a transmission electron microscope and x-ray diffraction. Dependence on TEM images and the predestined histogram (see Figure 5 (a-f) and see Figure 6 (a-f)), it is lucid that the average particle size equals 34 nm, 46 nm and 65 nm for Cobalt, Copper and Nickel complexes, respectively. Particle size of 25 nm, 42 nm and 16 nm was predestined for Co_3O_4 , CuO and NiO, respectively. These results manifest that the prepared compounds have great surface area and this can lead to many leader catalytic and potential properties.^[42] Figure 7 manifests the XRD modes of the synthesized CuO, Co_3O_4 and NiO nanoparticles. The data also affirm that the synthesized materials are CuO, Co_3O_4 and NiO, that all the diffraction peaks agreed with the reported standard data; no characteristic peaks were manifested other than metal oxides. The mean granule size (D) of the particles was predestined from the XRD line broadening measurement plying the Scherrer Equation^[43–48]:

$$D = 0.89\lambda/\beta \cos\theta \quad (7)$$

where λ is the wavelength (1.5406 Å), β is the full breadth

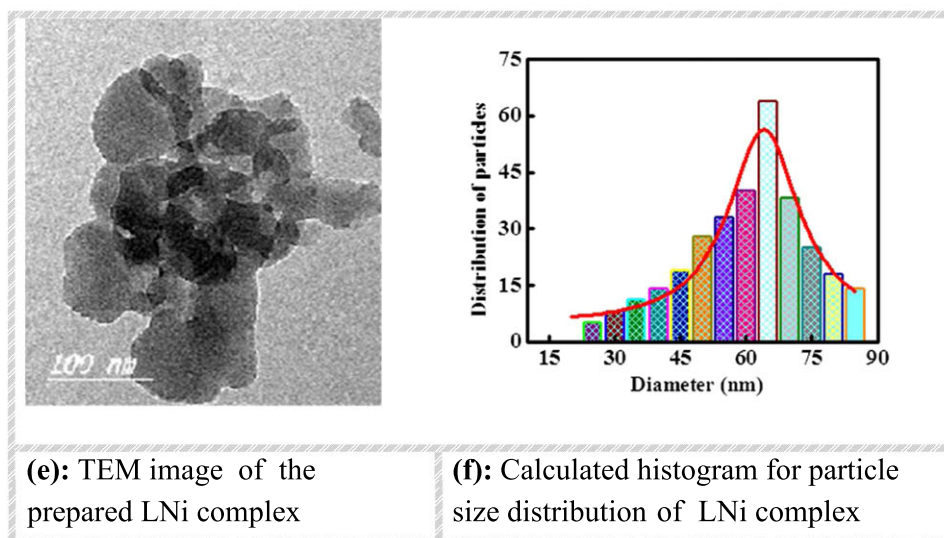
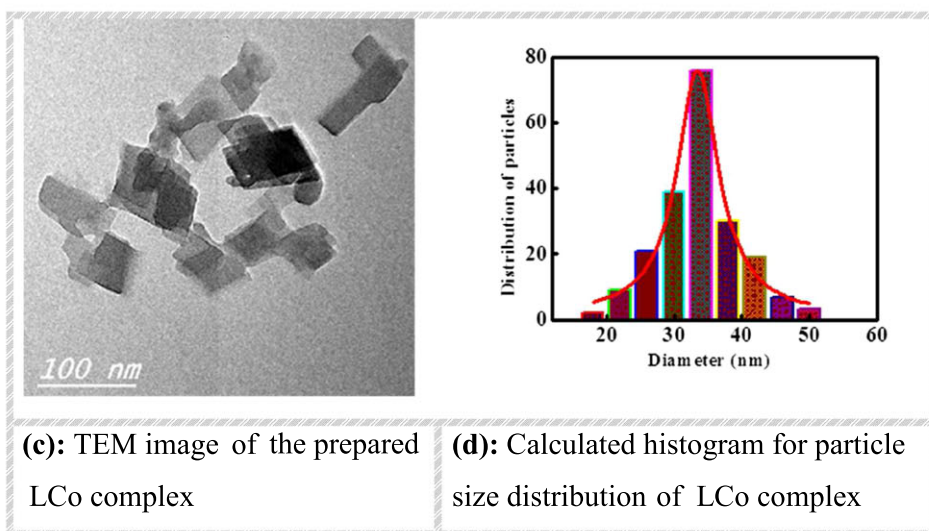
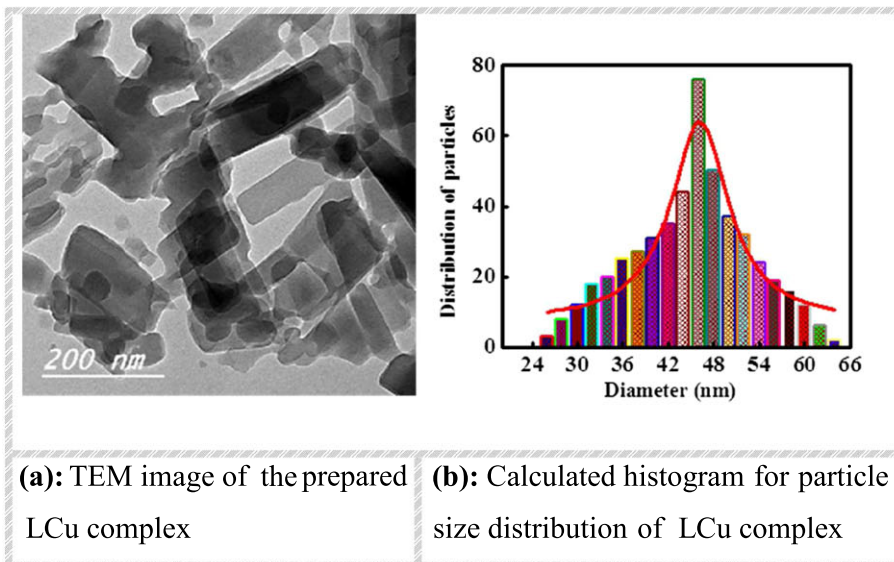


FIGURE 5 (a): TEM image of the prepared LCu complex, (b): Calculated histogram or particle size of LCu complex, (c): TEM image of the prepared LCo complex, (d): Calculated histogram for particle size distribution LCo complex, (e) TEM image of the prepared LNi complex, (f): Calculated histogram for particle size of LNi complex

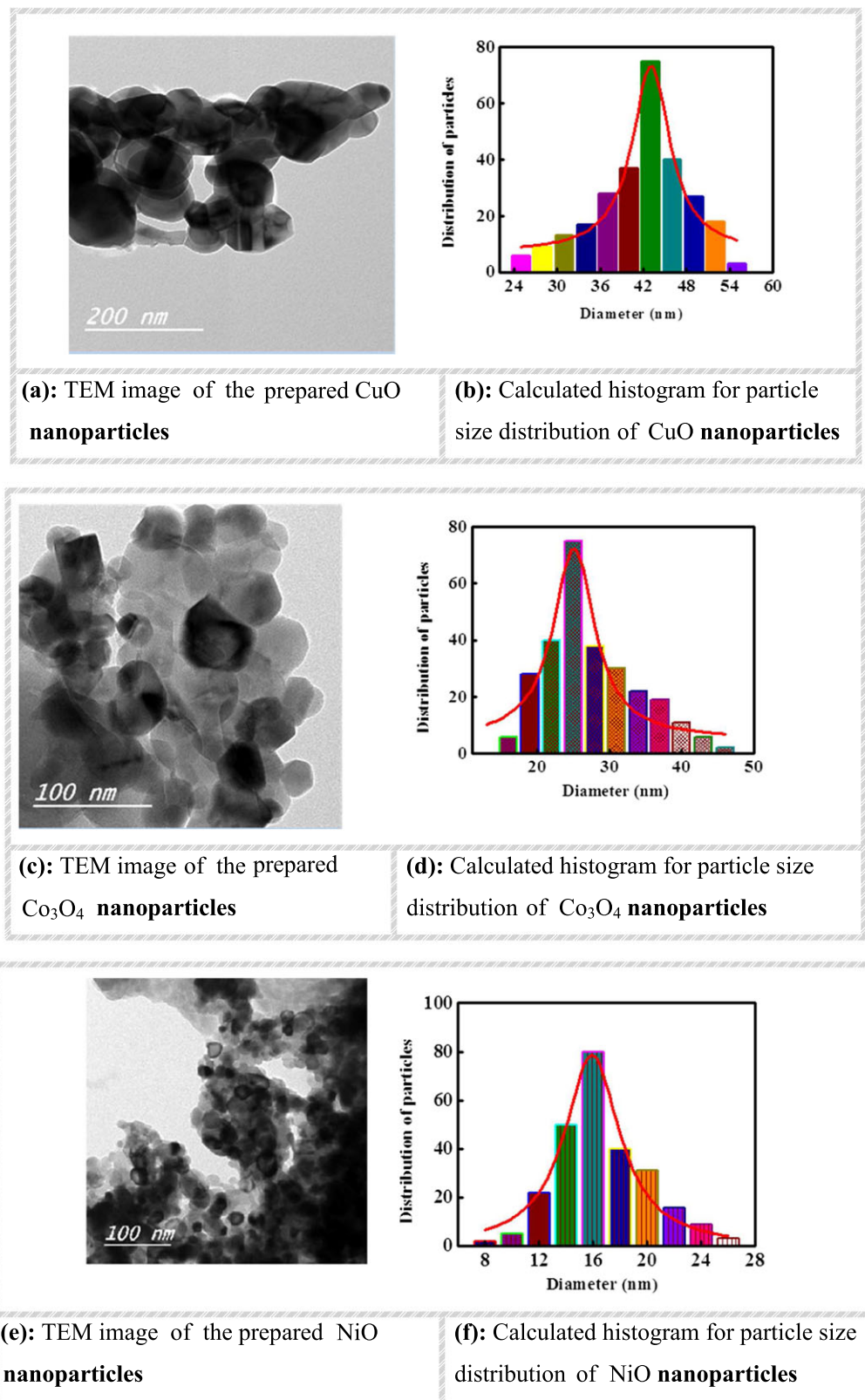


FIGURE 6 (a) TEM image of the prepared CuO nanoparticles, (b) Calculated histogram for particle size of CuO nanoparticles, (c) TEM image of the prepared Co_3O_4 nanoparticles, (d) calculated histogram for particle size of Co_3O_4 nanoparticles

at the half- maximum of the CuO, Co_3O_4 and NiO line and θ is the diffraction angle. Average crystallite size in

the domain of 16-46 nm were predestined for the CuO, Co_3O_4 and NiO nanoparticles.

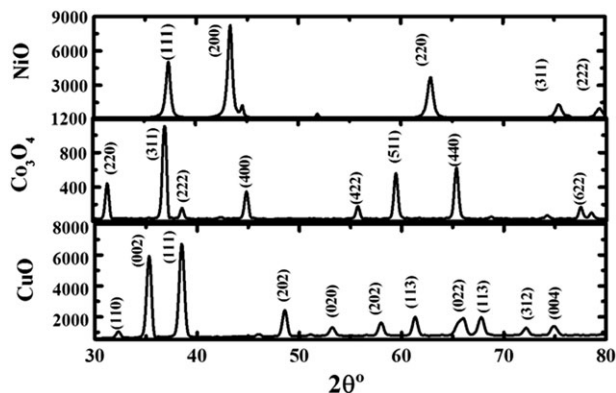


FIGURE 7 XRD patterns of CuO, Co₃O₄ and NiO nanoparticles

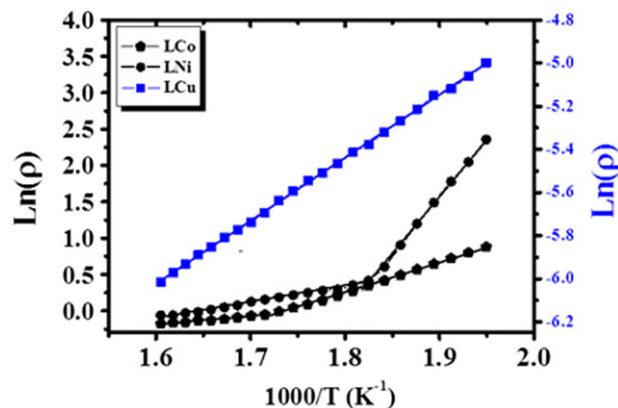


FIGURE 9 Ln(ρ) vs. 1000/T plots of the co, Ni and cu complexes

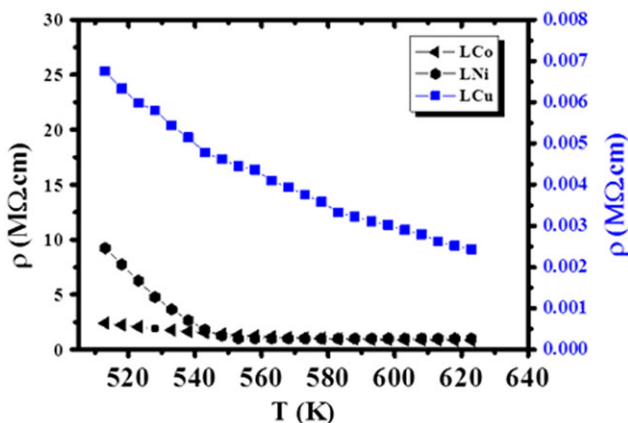


FIGURE 8 The temperature dependence of resistivity of the co, Ni and cu complexes

TABLE 3 Isothermal resistivity at 520 K ($\rho_{(520K)}$) and activation energies correspond to the inter-molecular (E_{aH}) and intra-molecular (E_{aL}) conduction of the complexes

Complex	E_{aL} (eV)	E_{aH} (eV)	$\rho_{(520K)}$ (MΩ.com)
Ni(II)	0.021	0.037	9.2
Co(II)	0.031	0.054	24.7
Cu(II)	0.017	--	0.063

4 | ELECTRICAL PROPERTIES

Figure 8 manifests the temperature reliance of resistivity of the Co(II), Ni(II) and Cu(II) complexes. As seen, the data reveal a semiconductor behavior where the resistivity decreases with the increases of temperature. The decrease of the electrical resistivity with increase of temperature is resulted from the increase of the charge carriers that can overcome the energy barrier and participate in the electrical conduction where in metal complexes, the metal atoms act as charge carriers reservoir supply the complex with the free electrons and the metal ion can act as a

bridge to facilitate the flow of current. To illustrate the effect of the metal type on the electrical resistivity of the ligand, isothermal resistivity values (determined at 520 K) of the all complexes are tabulated in Table 3. The data reveal that the resistivity can be tuned by choosing the proper metal for incorporation in the ligand. The ρ -T plots of Cobalt, Copper and Nickel complexes were found to be well represented by the well-known Arrhenius pattern which depicts the thermally activated conduction. According to this pattern, the resistivity reliance of temperature is depicted by the following relation:^[49]

$$\rho = \rho_0 \exp\left(\frac{E_a}{K_B T}\right) \quad (8)$$

Where E_a is the activation energy of conduction, K_B is the Boltzmann constant and ρ_0 is pre-exponential constant act the density of state and the charge carrier mobility. The activation energies of the conduction were predestined from the slope of the Ln(ρ) vs. 1000/T plots manifested in Figure 9. Noteworthy, the Ln(ρ) vs. 1000/T plots of the Co and Ni complexes manifest straight lines, each is

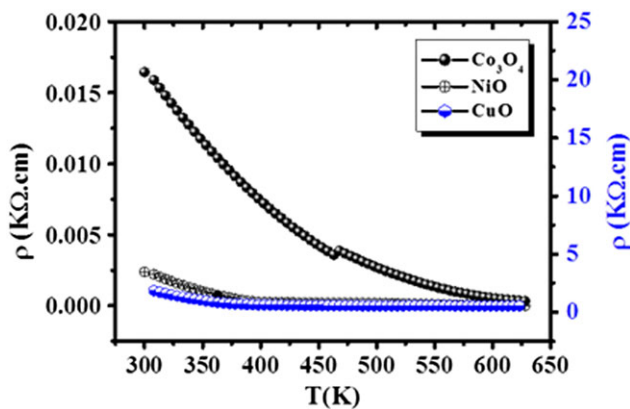


FIGURE 10 Temperature dependence of electrical resistivity of the metal oxides nanostructures

divided into two fractions with two slopes. This behavior affirms that the conduction in these complexes consists of two thermally activated mechanisms with two various activation energies. By taking in consider the structure of the complex, the conduction mechanisms can be explained reliance on two different transfer kinds of the charge carriers in the complex. The intra-molecular transfer, where the electrons hop from one atomic site to another if orbitals subsist at these sites are with the same energy levels i.e. the conduction procure due to the electron transfer between the ligand and the metal ions in the complex molecule. The other conduction mechanism, namely the intermolecular conduction, originates from the electron transfer between the neighboring complex molecules due to the overlapping of their molecular orbitals i.e. π -electrons can transmit from one macromolecule to another if orbitals with the same energy levels subsist between the complex molecules.^[50–53] Accordingly, the intermolecular

conduction can be assigned to the interaction between the electrons in d-orbitals of transition metal cations and the anti-bonding π -orbitals of the ligand.^[54] The intra-molecular conduction mechanism is described by lower activation energy E_{aL} compared to the activation energy of the intermolecular activation energy E_{aH} due to the tying of the excited free carriers within the molecule by the barriers macromolecules. The activation energies of the intermolecular and intra-molecular conduction mechanisms are patent in Table 3. Note that, the copper is characterized by one value of the activation energy. Thus, the conduction may be assigned to a combination of the two mechanisms simultaneously within the whole domain of the temperature of measurement without a domination of a certain one. The large change between activation energy values of the complexes may be due to contact resistance resulting from the various surface ratio of the three complexes.

Figure 10 shows the ρ - T plots of the metal oxides (Co_2O_3 , NiO and CuO) nanostructures. The data affirm that the materials have semiconductive properties where the resistivity reduces dramatically as the temperature raises. However, there is a clear difference between the isothermal resistivity values of the oxides. To be specific, the room temperature resistivity of Co_2O_3 , NiO, and CuO (ρ_{300}^{CoO} , ρ_{300}^{NiO} and ρ_{300}^{CuO}) where predestined to be 16.4, 2.3 and 1.1 $\Omega\cdot\text{cm}$. The semiconductor pattern of the samples under study is in well correspondance with the data published elsewhere.^[55–57] To grasp the electrical conduction mechanisms, various theoretical models were applied to the attained experimental data. It was found that, the pattern of the resistivity variation with temperature fits well with Equation 8. The well fit of the ρ - T data to Equation 8 is evidenced by the linear pattern of the $\text{Ln}(\rho)$ vs. $1000/T$ plots manifested in Figure 11. The plots depicted in Figure 11 allows predestin the activation energies E_a which were found to be 0.098 and 0.12 for Co and Cu oxides, respectively. These values are comparable to those published in other literature.^[55] Although the temperature reliance of the temperature of NiO nanoparticles exhibits typical semiconductor pattern like the other oxides under study, the ρ - T data do not fit well with Equation 9 where the accurate analyses affirm that the data are better represented by the following equation:

$$\rho/T = \rho_o e^{\frac{E_a}{k_B T}} \quad (9)$$

This pattern affirms that the conduction in the NiO oxide is band like type which can be assigned to the domination of the large polarons in the 2p band of O^{2-} .^[22,53] Activation energy value of 0.13 eV was predestined from temperature linear fits manifested in Figure 12 for the NiO nanoparticles which is comparable with values reported in other works.^[57]

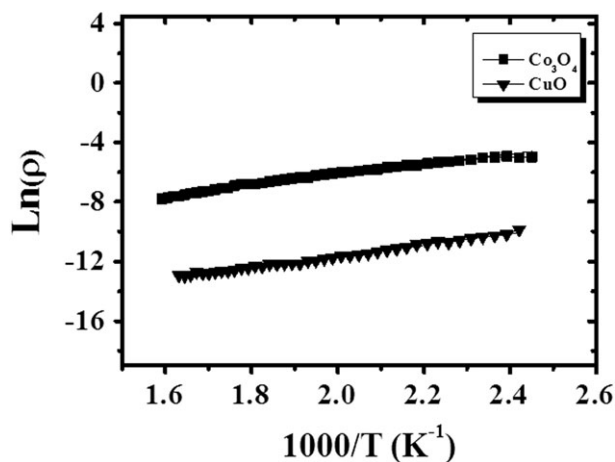


FIGURE 11 $\text{Ln}(\rho)$ vs. $1000/T$ for co and cu oxides nanostructures

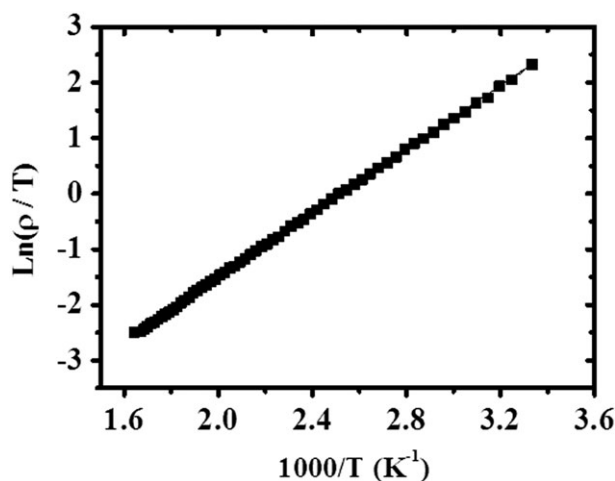


FIGURE 12 $\text{Ln}(\rho)$ vs. $1000/T$ for NiO nanoparticles

5 | CONCLUSION

The imine ligand was synthesized by the condensation of 2-amino-3-hydroxypyridine with 3-methoxysalicylaldehyde. The analytical data elucidates that the complexes have 1:1 (metal: ligand) stoichiometry. Conductivity measurements manifest their non-electrolytic kind. LH₂ ligand coordinates with the metal ions through the pyridyl-O, hydroxyl-O and azomethine-N. The ¹H-NMR data offer that the imine ligand deprotonated after complexation. Thermal data manifest degradation mode of the complexes. Thermo gravimetric mode of the complexes also assisted to describe the complexes. Nano-sized complexes were attained by ultrasonic irradiation in ethyl alcohol solution, and characterized by physico-chemical, XRD and TEM technicalities. Calcination under air of complexes outputs nano-sized metal oxides. The results of nanoparticle size measurement of specimens by XRD and TEM manifest that the size of the CuO, Co₃O₄ and NiO nanoparticles was about 16-46 nm. Moreover, the imine complexes and their corresponding metal oxides were manifested semiconductor pattern. The kind of metal has significant effect on the electrical resistivity of the complex. The conduction mechanism in the complexes is controlled by intra- and inter-molecular mechanisms of the charge carrier transfer. In the CuO, Co₃O₄ and NiO nanoparticles, the thermal activation conduction predominates. The charge carrier hopping mechanism is responsible of the conduction in the CuO and Co₃O₄ nanoparticles while the conduction in NiO nanoparticles is caused by small polaron hopping.

ORCID

Ahmed M. Abu-Dief  <http://orcid.org/0000-0003-3771-9011>

REFERENCES

- [1] L. H. Abdel-Rahman, R. M. El-Khatib, L. A. E. Nassr, A. M. Abu-Dief, *J. Mol. Struct.* **2013**, *1040*, 9.
- [2] L. H. Abdel-Rahman, R. M. El-Khatib, L. A. E. Nassr, A. M. Abu-Dief, M. Ismail, A. A. Seleem, *Spectrochim. Acta. A.* **2014**, *117*, 366.
- [3] A. M. Abu-Dief, I. M. A. Mohamed, *Beni-Suef Univ. J. Basic Appl. Sci.* **2015**, *4*, 119.
- [4] L. H. Abdel-Rahman, A. M. Abu-Dief, E. F. Newair, S. K. Hamdan, *J. Photochem. Photobiol. B.* **2016**, *160*, 18.
- [5] L. H. Abdel-Rahman, A. M. Abu-Dief, H. Mostafa, S. K. Hamdan, *Appl. Organometal. Chem.* **2017**, *31*, e3555.
- [6] A. S. Mocanu, M. Ilis, F. Dumitrascu, M. Ilie, V. Circu, *Inorg. Chim. Acta.* **2010**, *363*, 729.
- [7] A. M. Atta, N. O. Shaker, N. E. Maysour, *Prog. Org. Coat.* **2006**, *56*, 100.
- [8] J. H. Jia, X. M. Tao, Y. J. Li, W. J. Sheng, *Chem. Phys. Lett.* **2011**, *514*, 114.
- [9] A. M. Abu-Dief, M. S. M. Abdelbaky, D. Martínez-Blanco, Z. Amghouz, S. García-Granda, *Materials Chem. Physics* **2016**, *174*, 164.
- [10] A. M. Abu-Dief, I. F. Nassar, W. H. Elsayed, *Appl. Organometal. Chem.* **2016**, *30*, 917.
- [11] S. Kumar, D. N. Dhar, P. N. Saxena, *J. Sci. Ind. Res.* **2009**, *68*, 181.
- [12] K. C. Emregül, E. Düzgün, O. Atakol, *Corr. Sci.* **2006**, *48*, 3243.
- [13] J. Meyer, S. Hamwi, M. Kröger, W. Kowalsky, T. Riedl, A. Kahn, *Adv. Mater.* **2012**, *24*, 5408.
- [14] M. T. Greiner, M. G. Helander, W.-M. Tang, Z.-B. Wang, J. Qiu, Z.-H. Lu, *Nat. Mater.* **2012**, *11*, 76.
- [15] H. You, Y. Dai, Z. Zhang, D. Ma, *J. Appl. Phys.* **2007**, *101*, 026105.
- [16] M. Kroger, S. Hamwi, J. Meyer, T. Riedl, W. Kowalsky, A. Kahn, *Appl. Phys. Lett.* **2009**, *95*, 123301.
- [17] J. Meyer, M. Kroger, S. Hamwi, F. Gnam, T. Riedl, W. Kowalsky, A. Kahn, *Appl. Phys. Lett.* **2010**, *96*, 193302.
- [18] J. Manna, G. Begum, K. Pranay Kumar, S. Misra, R. K. Rana, *ACS Appl. Mater. Interfac.* **2013**, *5*, 4457.
- [19] L. H. Abdel-Rahman, A. M. Abu-Dief, R. M. El-Khatib, S. M. Abdel-Fatah, *Bioorg. Chem.* **2016**, *69*, 140.
- [20] L. H. Abdel-Rahman, A. M. Abu-Dief, S. K. Hamdan, A. A. Seleem, *Int. J. Nano. Chim.* **2015**, *1*, 65.
- [21] L. H. Abdel-Rahman, A. M. Abu-Dief, M. S. S. Adam, S. K. Hamdan, *Catal. Lett.* **2016**, *146*, 1373.
- [22] S. A. Ahmed, E. M. M. Ibrahim, S. A. Saleh, *Appl. Physics. A.* **2006**, *85*, 177.
- [23] L. H. Abdel-Rahman, A. M. Abu-Dief, R. M. El-Khatib, S. M. Abdel-Fatah, *J. Photochem. Photobiol. B.* **2016**, *162*, 298.
- [24] L. H. Abdel-Rahman, R. M. El-Khatib, L. A. E. Nassr, A. M. Abu-Dief, F. E.-D. Lashin, *Spectrochim. Acta. A.* **2013**, *111*, 266.
- [25] A. M. Abu-Dief, L. A. E. Nassr, *J. Iran. Chem. Soc.* **2015**, *12*, 943.
- [26] A. M. Abu-Dief, R. Díaz-Torres, E. C. Sañudo, L. H. Abdel-Rahman, N. A. Alcalde, *Polyhedron* **2013**, *64*, 203.
- [27] L. H. Abdel-Rahman, A. M. Abu-Dief, N. M. Ismail, M. Ismael, *Inorg. and Nano-Metal Chem.* **2017**, *47*, 467.
- [28] H. Abdel-Rahman, A. M. Abu-Dief, M. Ismael, M. A. A. Mohamed, N. A. Hashem, *J. Mol. Struct.* **2016**, *1103*, 232.
- [29] R. A. Kusanur, M. Ghate, M. V. Kulkarni, *J. Chem. Sci.* **2004**, *116*, 265.
- [30] L. H. Abdel-Rahman, N. M. Ismail, M. Ismael, A. M. Abu-Dief, E. Abdel-Hameed Ahmed, *J. Mol. Struct.* **2017**, *1134*, 851.
- [31] L. H. Abdel-Rahman, R. M. El-Khatib, L. A. E. Nassr, A. M. Abu-Dief, *Arab. J. Chem.* **2017**, *10*, S1835.
- [32] L. H. Abdel Rahman, A. M. Abu-Dief, N. A. Hashem, A. A. Seleem, *Int. J. Nano. Chem.* **2015**, *1*, 79.

- [33] LH Abdel-Rahman, AM Abu-Dief, H Moustafa, AAH Abdel-Mawgoud, Arab. J. Chem. **2017**, <https://doi.org/10.1016/j.arabjc.2017.07.007>
- [34] M. Shakir, S. Hanif, M. A. Sherwani, O. Mohammad, M. Azam, S. I. Al-Resayes, *J. Photochem. Photobiol. B: Bio.* **2016**, 157, 39.
- [35] E.-H. M. Diefallah, *Acta.* **1992**, 202, 1.
- [36] 285L. H. Abdel-Rahman, A. M. Abu-Dief, M. O. Aboelez, A. A. Hassan Abdel-Mawgoud, *J. Photochem. Photobiol. B.* **2017**, 170, 271.
- [37] L. H. Abdel-Rahman, A. M. Abu-Dief, M. Basha, A. A. H. Abdel-Mawgoud, *Appl. Organomet. Chem.* **2017**, 31, e3750.
- [38] L. H. Abdel-Rahman, R. M. El-Khatib, L. A. E. Nassr, A. M. Abu-Dief, *Inter. J. Chem. Kin. A.* **2014**, 46, 543.
- [39] H. M. Abd El-Lateef, A. M. Abu-Dief, B. E. M. El-Gendy, *J. Electroanal. Chem.* **2015**, 758, 135.
- [40] H. M. Abd El-Lateef, A. M. Abu-Dief, M. A. A. Mohamed, *J. Mol. Struct.* **2017**, 1130, 522.
- [41] H. M. Abd El-Lateef, A. M. Abu-Dief, L. H. Abdel-Rahman, E. C. Sañudo, N. Aliaga-Alcalde, *J. Electroanal. Chem.* **2015**, 743, 120.
- [42] M. A. E. A. A. Ali El-Remaily, A. M. Abu-Dief, *Tetrahedron* **2015**, 71, 2579.
- [43] P. Scherrer, *Göttinger Nachrichten Gesell.* **1918**, 2, 98.
- [44] E. M. M. Ibrahim, S. Hampel, R. Kamsanipally, J. Thomas, K. Erdmann, S. Fuessel, C. Taeschner, V. O. Khavrus, T. Gemming, A. Leonhardt, B. Buechner, *Carbon* **2013**, 63, 358.
- [45] T. Jaumann, E. M. M. Ibrahim, S. Hampel, D. Maier, A. Leonhardt, B. Büchner, *Chemical Vapor Deposition* **2013**, 19, 228.
- [46] M. A. A. El-Remaily, A. M. Abu-Dief, R. M. El-Khatib, *Appl. Organometal. Chem.* **2016**, 30, 1022.
- [47] A. M. Abu-Dief, W. S. Mohamed, *Mater. Res. Express* **2017**, 4, 035039.
- [48] A. A. Marzouk, A. M. Abu-Dief, A. A. Abdelhamid, *Appl Organometal Chem.* **2017**, e3794. <https://doi.org/10.1002/aoc.3794>.
- [49] M. M. Ibrahim, E. M. M. Ibrahim, S. A. Saleh, A. M. A. Hakeem, *J. Alloys Compd.* **2007**, 429, 19.
- [50] F. Gutmann, *Organic Semiconductors*, John Wiley Sons Inc., NewYork, London, Sydney **1967**.
- [51] N. F. Mott, E. A. Davis, *Electronic Processes in Non-crystalline Materials*, Clarendon Press, Oxford **1971**.
- [52] T. H. Scabarozzi, S. Amini, P. Finkel, O. D. Leaffer, J. E. Spanier, M. W. Barsoum, M. Drulis, H. Drulis, W. M. Tambussi, J. D. Hettinger, S. E. Lofland, *J. Appl. Phys.* **2008**, 104, 3350.
- [53] M. G. Abd el wahed, S. A. Aly, H. A. Hammad, S. M. Metwally, *J. Phys. Chem. Solids.* **1994**, 55, 31.
- [54] M.-T. Chang, L.-J. Chou, C.-H. Hsieh, Y.-L. Chueh, Z.-L. Wang, Y. Murakami, D. Shindo, *Adv. Mater.* **2007**, 19, 2290.
- [55] E. M. M. Ibrahim, *Appl. Phys. A.* **2007**, 89, 203.
- [56] E. M. M. Ibrahim, A. M. Abu-Dief, A. Elshafaie, A. M. Ahmed, *Mat. Chem. and Phys.* **2017**, 192, 41.
- [57] D. Adler, J. Feinleib, *Phys. Rev. B.* **1970**, 2, 3112.

SUPPORTING INFORMATION

Additional Supporting Information may be found online in the supporting information tab for this article.

How to cite this article: Abdel Rahman LH, Abu-Dief AM, El-Khatib RM, Abdel-Fatah SM, Adam AM, Ibrahim EMM. Sonochemical synthesis, structural inspection and semiconductor behavior of three new nano sized Cu(II), Co(II) and Ni(II) chelates based on tri-dentate NOO imine ligand as precursors for metal oxides. *Appl Organometal Chem.* 2017;e4174. <https://doi.org/10.1002/aoc.4174>